Thin Solid Films 570 (2014) 429–435

Contents lists available at ScienceDirect

Thin Solid Films

journal homepage: www.elsevier.com/locate/tsf

In-situ doping of erbium in hydrogenated amorphous carbon by low temperature metalorganic radio frequency plasma enhanced chemical vapor deposition

Hui-Lin Hsu [a,*], Keith R. Leong [a], Michael Halamicek [a], I-Ju Teng [b,c], Pratish Mahtani [a], Jenh-Yih Juang [b,c], Sheng-Rui Jian [d], Li Qian [a], Nazir P. Kherani [a,e,**]

[a] Department of Electrical and Computer Engineering, University of Toronto, ON M5S 3G4, Canada
[b] Centre for Interdisciplinary Science, National Chiao Tung University, Hsinchu 30010, Taiwan
[c] Department of Electrophysics, National Chiao Tung University, Hsinchu 30010, Taiwan
[d] Department of Materials Science and Engineering, I-Shou University, Kaohsiung 84001, Taiwan
[e] Department of Materials Science and Engineering, University of Toronto, ON M5S 3E4, Canada

ARTICLE INFO

Available online 15 February 2014

Keywords:
Erbium metalorganic compound
Hydrogenated amorphous carbon (a-C:H)
Fluorination

ABSTRACT

A significant improvement in the photoluminescence of erbium doped amorphous carbon (a-C:H(Er)) is reported. The effects of the RF power on the anode and cathode a-C:H films were investigated in terms of the microstructural and local bonding features. It was determined that Er doped a-C:H films should be placed on the anode to obtain wider bandgap and lower percentage of sp^2 carbon bonding. The metalorganic compound, tris(6,6,7,7,8,8,8-heptafluoro-2,2-dimethyl-3,5-octanedionate) Erbium(+III) or Er(fod)$_3$, was incorporated in-situ into an a-C:H host by metalorganic rf plasma enhanced chemical vapor deposition. This technique provides the capability of doping Er in a vertically uniform profile. The high erbium concentration (3.9 at.%), partial fluorination of the surrounding ligands, and the large optical bandgap of the host a-C:H are the primary factors that enable enhancement of the photoluminescence.

1. Introduction

The metal-line based electrical interconnections represent the most important limitation on the performance of Si-based microelectronic (CMOS) devices. The delay in the signal propagation arises from several factors including the parasitic capacitances generated at the metal/insulator/metal capacitors, the intrinsic resistivity of the metal lines, and the contact resistance at the metal/metal interface. As device features further shrink, the delay due to the metal interconnection will lead to an unacceptable bottleneck in device performance [1]. A definitive solution is to employ optical interconnects that are able to transfer data at rates that are orders of magnitude above the limit of traditional electronic technologies. These optical interconnects can be inside a Si chip or between chip-to-chip communication. In order to completely avail optical technologies, it is imperative to develop silicon compatible materials which enable light generation, guiding, switching, detection, modulation and amplification. To realize the co-existence of electrical and optical functions inside a Si chip platform, it is crucial to develop compatible photonic materials. These materials must possess processing temperatures below 400 °C, in order to meet the Si back end-of-line (BEOL) requirements for the current integrated circuit (IC) fabrication technology.

The development of Si compatible photonic materials includes the observation of an optical gain in Si nanocrystals [2], electroluminescence for a Si diode [3], Si nanocrystal field-effect-transistors [4], implementation of a Si Raman laser [5], and the realization of a high-speed Si electro-optic modulator [6]. However, given silicon's inherent indirect bandgap, crystalline Si is not able to readily emit light. This limits the approaches described above. Thus the lack of an efficient Si-based light source is self-evident.

Erbium (Er) ion implantation in a variety of Si-based [7–9], silica-based [8,10], and ceramic [8] thin film hosts has a leading role in the effort to efficiently produce photons from Si. The advantage of this approach is that standard Si technology can be deployed to introduce Er as a dopant. In addition, excited Er^{3+} ions emit at 1.5 μm, which is a strategic wavelength for telecommunications due to the minimum in the absorption for silica fibers. However, photoluminescence is severely quenched at room temperature in crystalline Si based hosts [11,12]. Also, co-implantation of additional O atoms is highly preferred in order to reduce Er precipitation and increase the fraction of active Er^{3+} ions [13]. For silica-based and ceramic thin film hosts, a high processing temperature is required to grow good quality material. Also,

* Corresponding author.
** Correspondence to: N.P. Kherani, Department of Electrical and Computer Engineering, University of Toronto, ON M5S 3G4, Canada.
E-mail addresses: l.qian@utoronto.ca (L. Qian), kherani@ecf.utoronto.ca (N.P. Kherani).

http://dx.doi.org/10.1016/j.tsf.2014.02.038
0040-6090/

high post-annealing temperatures (>700 °C) are typically necessary to eliminate the ion implantation-induced damage, to optically activate the Er^{3+} ions, and/or to enhance the photoluminescence lifetime or quantum efficiency. These high temperature processes are incompatible with Si BEOL fabrication processes.

While research on Er-implanted silicon and silica-based materials has been extensive, Er doping in amorphous carbon based host has received little attention [14–17]. Hydrogenated amorphous carbon (a-C:H) films can be grown by a low-temperature plasma enhanced chemical vapor deposition (PECVD) method. PECVD methods are compatible with current CMOS fabrication technology. They allow ease of integration and reproducible processing, and are low-cost. Furthermore, a-C based films possess a number of outstanding properties such as high chemical resistance, biocompatibility, mechanical hardness, and transparency in the infrared [18,19]. Due to their excellent tribological properties, a-C:H films are widely used as protective coatings for hard disks and magnetic media, machine parts, optical windows and fibers, etc. [20]. In the past few years, a-C:H coatings have been also implemented on biomedical and biosensor products [21]. The specific properties of a-C:H films can be tailored over a wide range by adjusting the sp^3 to sp^2 hybridized carbon ratio, the type of sp^3 (predominately C – C or a mixture of C – C and C – H) and sp^2 (the number and size of the clusters) bonding configurations, and the amount of incorporated hydrogen in the film via various deposition parameters and deposition methods [19].

The first reported demonstration of room-temperature photoluminescence (PL) from Er at 1.54 μm in a-C:H(Er) thin films was published in 2002 [14]. a-C:H(Er) films were deposited by magnetron sputtering of a graphite target that was partially covered by Er platelets in an Ar/C_6H_{12} atmosphere. The Er concentration in the a-C:H(Er) films could be changed from 0.15 at.% to 1.2 at.%. However, the PL intensity was relatively low. This was attributed to the low optical band gap (~0.5 eV) of the sample and the non-radiative relaxation pathway induced by C – H vibrations [15]. In this deposition technique, the Er concentration highly depends on the degree of magnetron sputtering of the Er/graphite target. Accordingly, high Ar ion energy and flux are required to achieve high Er concentration. However, this causes a high concentration of sp^2 carbon and a low optical bandgap. The incorporation of an Er metalorganic compound into a carbon layer by the radio frequency plasma enhanced chemical vapor deposition (RFPECVD) method was demonstrated by Prajzler et al. [16] in 2003. However no PL spectra were presented. In 2009, Tsai et al. [17] grew a-C:H(Er) and a-C:D(Er) films, where D in a-C:D(Er) is deuterium, the isotope of H, via in-situ thermal evaporation of the tris(2,2,6,6-tetramethyl-3-5 heptanedionato) erbium(+III), or $Er(tmhd)_3$, compound in a DC saddle-field PECVD system. A much higher PL signal was obtained from a-C:D(Er) film compared to a-C:H(Er) films. This was due to the optical quenching from the highly abundant C – H bonds. The $Er(tmhd)_3$ metalorganic compound contains a high percentage of C – H bonds, 58.76 at.%. Hence, this precursor is inherently inefficient at promoting Er^{3+} photoluminescence.

In this work, the feasibility of the in-situ growth of metalorganic Er-doped amorphous carbon (a-C:H(Er)) thin films was performed. Films were deposited at low temperature (<200 °C) by a metalorganic radio frequency plasma-enhanced chemical vapor deposition (MO-RFPECVD) system. The properties of the host a-C:H film and the incorporated Er concentration were independently controlled. Prior to the MO-RFPECVD depositions, the effects of the RF power and the placement of substrate in the RFPECVD system were systematically investigated. The structural and optical properties of the host a-C:H material were obtained. These properties were evaluated and discussed with respect to the local bonding features.

2. Experimental details

2.1. MO-RFPECVD and sample preparation

A capacitively coupled MO-RFPECVD system as shown in Fig. 1 was deployed to deposit hydrogenated amorphous carbon (a-C:H) and Er-doped a-C amorphous carbon (a-C:H(Er)) thin films. An ac-powered thermal evaporator was situated next to the RF-powered showerhead electrode (cathode) inside the deposition chamber. The thermal evaporator was used to in-situ dope the Er metalorganic compound while commencing a-C:H film deposition via a methane plasma. A thermocouple was embedded in the external surface of the bottom of the evaporator for feedback temperature control. This measured temperature was

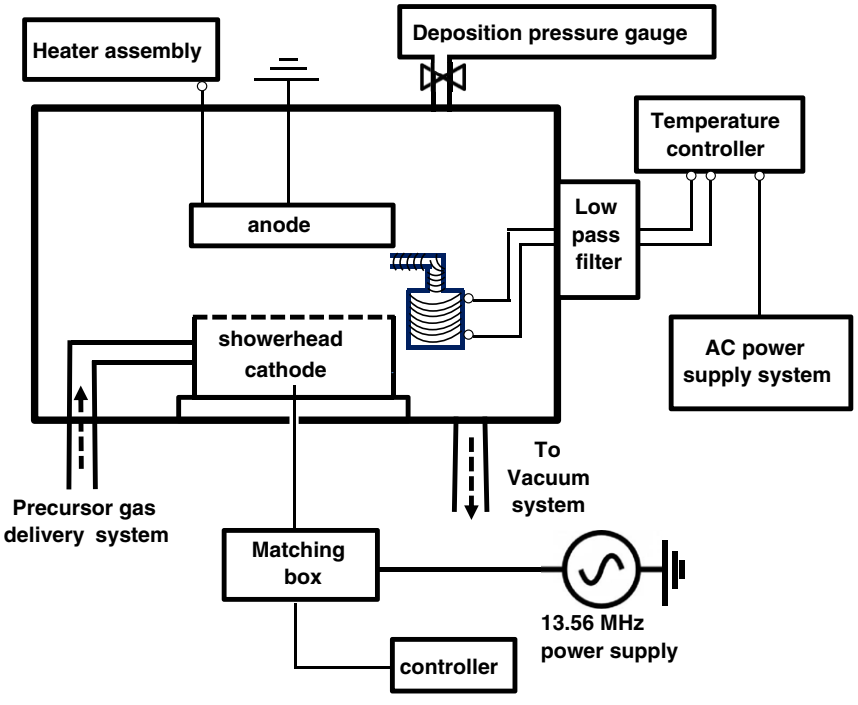

Fig. 1. Schematic diagram of the MO-RFPECVD system used for the preparation of a-C:H(Er) films.

designated as the nominal evaporator temperature. The temperature of the vapor delivery nozzle was also measured and found to be higher than that of the external bottom surface of the container by 30–50 °C. This temperature difference prevented condensation of the Er metalorganic vapor on the delivery nozzle. Further, it is expected that the temperature inside the container is higher than the evaporation temperature thus enabling the observed sublimation of the Er metalorganic powder. For a-C:H films, the methane (CH_4) flow rate was 40 sccm and the chamber pressure was 16 Pa. The substrates were kept at room temperature, while the RF power was varied from 10 W to 300 W. For the a-C:H(Er) sample, the evaporation temperature was 150 °C. The substrate temperature of 80 °C was used, as opposed to room temperature, so as to aid the uniformity of the prepared films as well as to avoid the direct condensation of the metalorganic vapor in powder form; precluding direct condensation ensures vapor-plasma chemistry leading to molecular occlusion of the dopant. The RF power was selected to be 40 W so as to minimize the sp^2 content in the host a-C:H film, and to lower the probability of dissociating the Er – O bonds in the pristine metalorganic compound due to energetic ions/radicals. The flow rate and pressure was the same as that for the a-C:H films. The c-Si substrates with resistivity of 30 Ω-cm were subjected to the standard CMOS cleaning procedure before being loaded into the chamber.

2.2. Er metalorganic compound

$Er(tmhd)_3$ powder has been used as precursor in a-Si:H(Er) samples prepared by PECVD [22]. The Er in $Er(tmhd)_3$ is coordinated to six oxygen atoms, which represents a similar bonding environment to Er_2O_3. This bonding environment is thought to be replicated in the a-Si:H(Er) samples since the Er acted as an optically emitting center [22]. Herein, a similar compound, tris(6,6,7,7,8,8,8-heptafluoro-2,2-dimethyl-3,5-octanedionate) Erbium(+III), abbreviated ($Er(fod)_3$), with chemical structure $Er(C_{10}H_{10}F_7O_2)_3$, as represented in Fig. 2, is selected as the doping candidate for a-C:H(Er) films in this work. The $Er(fod)_3$ powder was obtained from Strem Chemicals Inc. and was loaded into the vacuum chamber without any special treatment. The Er in $Er(fod)_3$ also has a similar bonding environment to Er_2O_3. Moreover, the large separation of the Er ions is expected to reduce concentration quenching. Furthermore, the fluorinated ligands are expected to reduce the non-radiative deactivation channels from C – H bonds. This will enable an enhancement in the Er^{3+} luminescence efficiency [23,24].

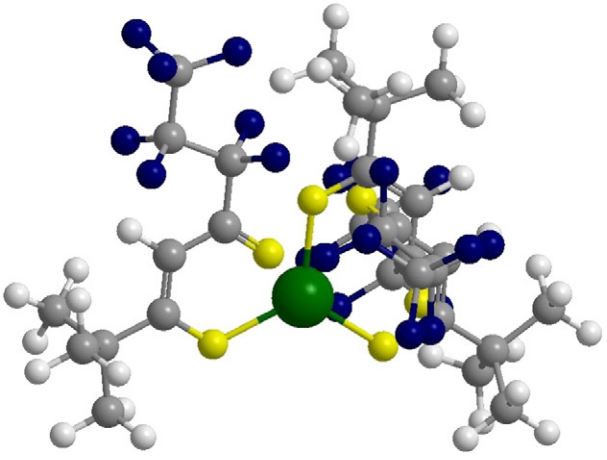

Fig. 2. Illustration of the Er metalorganic compound, $Er(fod)_3$, with chemical structure $Er(C_{10}H_{10}O_2F_7)_3$. The large center green atom represents Er, yellow atoms represents O, the dark gray atoms represent C, blue atoms represent F, and white atoms represent H.

2.3. Film characterization

The thickness (deposition rate), refractive index n, extinction coefficient k, and optical bandgap E_{04} of the a-C:H films were probed through spectroscopic ellipsometry. The measurements were carried out using a Sopra UV–VIS-NIR spectroscopic ellipsometer. The wavelength range was 350–1700 nm at an incident angle of 75°. The spectra were analyzed by regression fitting using the linear Levenberg–Marquard algorithm method with a maximum of 1000 iterations under a three-layer optical system, void (ambient)/a-C:H layer/c-Si substrate. A first-order initial thickness approximation of the a-C:H film was estimated from profilometry measurements. The five constants of Forouhi–Bloomer dispersion model [25] and thickness of the a-C:H layer were allowed to vary during the fitting process. The optical bandgap E_{04}, defined as the photon energy at which the absorption coefficient $\alpha(=4\pi k/\lambda)$ is equal to 10^4 cm^{-1},where λ is the wavelength, was determined from the extinction coefficient k. The coefficient of regression R^2 ~0.99, and the error of the 6 fitting parameters was less than +/− 10% indicating the model was appropriate for the a-C:H films.

The hydrogen concentration and $C-H_x$ stretching absorption bands were characterized by Fourier Transform Infra-Red (FTIR) Spectroscopy using a Perkin Elmer 2000 spectrometer with the resolution of 4 cm^{-1}. To calculate the transmission spectra from the thin film alone, the background interference pattern due to the multiple reflections in the film was subtracted from the raw transmission spectra. The hydrogen concentration was determined by the following equation [26]

$$H.conc. = \frac{A_s(CH_x)}{<\upsilon>}\int a(\nu)\ d\nu \tag{1}$$

where $\alpha(\upsilon)$ is the absorption coefficient, $A_s(CH_x)$ is the absorption cross section of individual stretching mode and $<\upsilon>$ is the average wavenumber. The IR spectrum in the wavenumber region 2700–3100 cm^{-1} was deconvoluted based on the various bond assignments and their corresponding wavenumber. $A_s(CH_x)$ was calculated by considering the cross section in a vacuum environment and extrapolation refractive index n of each sample to 3.3 μm [26].

X-ray photoelectron spectroscopy (XPS) was used to quantitatively characterize the elemental composition, bonding configuration, and the depth distribution of the a-C:H and a-C:H(Er) films. The XPS was a Thermo Fisher Scientific K-Alpha spectrometer with a monochromatic Al Kα X-ray source. The base pressure of the XPS was of order of 10^{-7} Pa. X-ray excited auger electron spectroscopy (XAES) was employed to estimate the ratio between the sp^2-hybridized and sp^3-hybridizd carbon atoms in the host a-C:H films. The percentage of sp^2 hybridized carbon is found through Eq. (2) [27]

$$\%sp^2 = \frac{\left(D_{sample} - D_{diamond}\right)}{\left(D_{graphite} - D_{diamond}\right)} \times \ 100\,\% \tag{2}$$

where D-parameter can be found in the derivative spectra of XAES measurements.

Photoluminescence (PL) spectra of a-C:H(Er) films were collected at room temperature to verify the optical activity of the Er in the a-C:H(Er) films. A continuous wave diode-pumped solid-state 532 nm laser, with a power density of 80 mW/mm^2, was used as the excitation source. The energy of the laser is nearly resonant with the $^4S_{3/2}$ excited level of the Er ions. The excited Er ions decayed to the $^4I_{13/2}$ level through a fast non-radiative transition, and then a photon is emitted at 1.54 μm through the $^4I_{13/2}$ to $^4I_{15/2}$ transition. A single pass monochromator, thermoelectrically cooled InGaAs photodiode, and a standard lock-in amplifier were used.

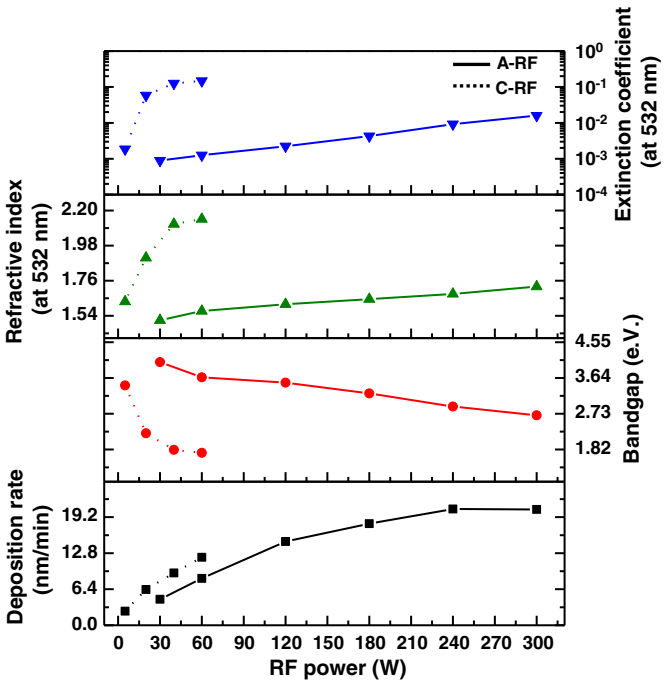

Fig. 3. The optical properties (E_{04}, n, k) and deposition rate of a-C:H films grown on the anode (solid line), and cathode (dash line), as a function of the applied RF power.

3. Results and discussion

3.1. a-C:H host

Fig. 3 reveals the dependence of deposition rate, optical bandgap E_{04}, refractive index n and extinction coefficient k on the applied RF power for the a-C:H films grown on the bottom powered (cathode, i.e. C-RF) and top grounded (anode, i.e. A-RF) electrodes respectively. Both of the sample sets, C-RF and A-RF, reveal similar trends of an increase in the deposition rate, decrease in the optical bandgap E_{04}, increase in the refractive index and extinction coefficient with increasing RF power. However, the rate of change of n and k at 532 nm and E_{04} is more rapid for the C-RF sample set. This indicates that the placement of substrate in this work plays an important role in the film deposition process.

The deconvoluted FTIR absorption spectra, normalized on the film thickness, provide insight into the presence of the different $C-H_x$ stretching modes in terms of the hybridization and bond configurations in the a-C:H films. Nine C – H stretching modes have been identified through examination of free molecule vibrational frequencies which comprises the absorption spectra from 2700 cm^{-1} to 3100 cm^{-1} and can be found in Ristein [26]. Fig. 4(a) and (b) displays the IR absorption coefficient for the a-C:H films grown on the anode and cathode with an RF power of 60 W. For the film grown on the anode in Fig. 4(a), there is a wide range of stretching modes. In particular, there is a significant contribution from the end groups sp^3CH_3 and sp^3CH_2 with an estimated concentration (from Eq. (1)) of 1.78×10^{22} and 7.75×10^{21} cm^{-3}. In contrast, for the film grown on the cathode in Fig. 4(b) there is a comparable amount in sp^3CH_2 (6.82×10^{21} cm^{-3}), sp^2CH olefinic (3.12×10^{21} cm^{-3}), and sp^2CH aromatic (5.18×10^{21} cm^{-3}). The total hydrogen concentration of the a-C:H films decreases with increasing RF power as displayed in Fig. 4(c). Moreover, the hydrogen concentration is lower for the a-C:H films deposited on the cathode. As well, for the films on the cathode, there is larger rate of decrease of the hydrogen concentration with increasing RF power.

As the RF power is increased there is a corresponding increase in the RF voltage and current. This increases the ion energy and the plasma density, and hence there is more ionization, excitation, and dissociation. This leads to an increase in the flux of ions, radicals, and electrons to the substrate surface which corresponds to an increase in the deposition

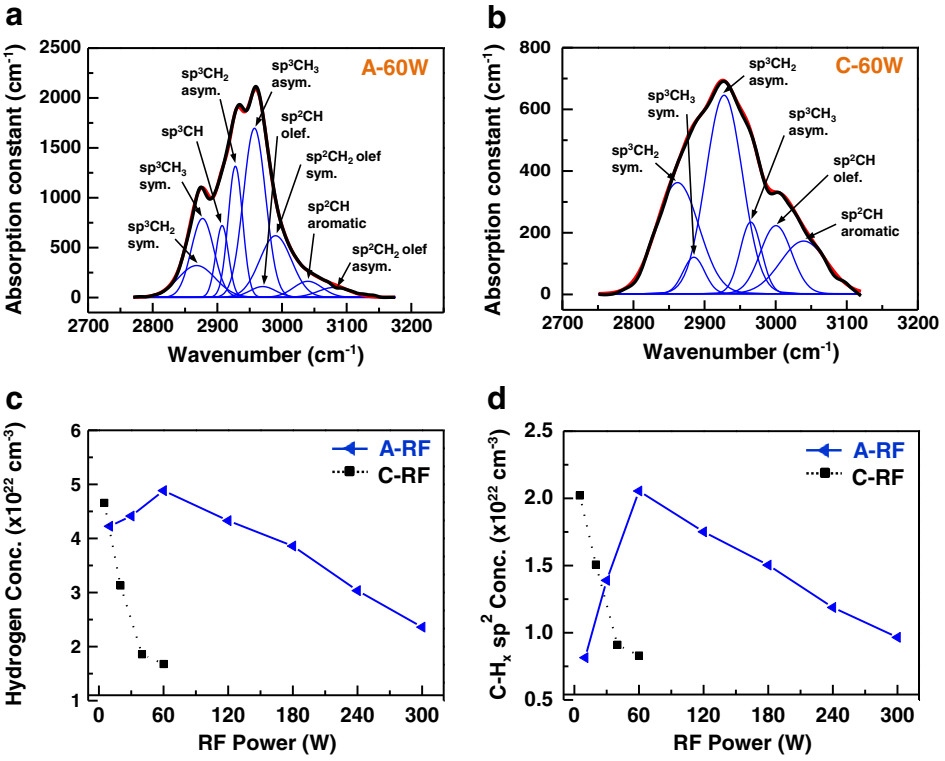

Fig. 4. Deconvoluted FTIR spectra in the $C-H_x$ stretching region for a-C:H films grown at an RF power of 60 W on the (a) anode and (b) cathode, respectively. (c) The hydrogen concentration and (d) the $C-H_x$ sp^2 bonding concentration as a function of the applied RF power for a-C:H films grown on the anode (solid line) and on the cathode (dash line).

rate for both the cathode and the anode. The deposition rate in the C-RF sample set is 10–15% higher than that in the A-RF sample set. This is attributed to the larger area of the electrically grounded surface and to the higher ion/radical energy impinging on the cathode. In a capacitively coupled RFPECVD system, any asymmetry in the sheath capacitances (anode and cathode) results in a DC bias on the electrodes. Typically, and in the present case, the anode is grounded and the cathode is smaller than the anode. Since the capacitance varies with the electrode area, and the voltage across a capacitor is inversely proportional to its capacitance, a DC bias is developed on the smaller electrode, the cathode. Hence, the ions and radicals impinging on the cathode possess greater energy than those impinging on the anode. These higher energy ions and radicals can penetrate the surface of a growing film and bond to a carbon cluster within the bulk of the film, leading to a higher growth rate.

As the RF power increases the ion energy increases since the RF voltage increases. As well, the DC bias on the cathode is increased from 34 V to 543 V with increasing RF power from 10 W to 300 W. Thus, ions striking the cathode possess a great deal and more energy than those striking on the anode. The increase in ion energy with RF power accounts for the decreasing trend of the hydrogen concentration in the a-C:H film. High energy hydrogen ions/radicals can penetrate into the bulk of the film to displace a bonded hydrogen atom, form H_2, and desorb from the film [19]. Nevertheless, for the A-RF sample set the hydrogen concentration initially increases then decreases with a peak at 30 W. This is thought to be due to the increased plasma density as the RF power is increased from 10 W to 30 W. Although the film density is not taken into account, it is recognized that a relatively low hydrogen atomic density (in atoms/cm^3) may actually be transformed into a relatively high atomic percentage (in at.%) if the film exhibits a low density. Moreover, the C – H_x sp^2 bonding modes could provide a qualitative measure of the change in the relative H bonding configuration with RF power. Hydrogen prefers to bond to sp^3 hybridized carbon atoms as it represents a lower energy state than sp^2 hybridized carbon. Accordingly, the C – H_x sp^2 would be less likely to occur unless the available sp^3 carbon bonds are near saturation due to a high percentage of hydrogen in the film. As depicted in Fig. 4(d), the C – H_x sp^2concentration also tends to decrease as RF power increases except for the A-RF sample set with low power. Furthermore, the rate of decline of the H concentration and the C – H_x sp^2 concentration is significantly larger for the C-RF sample set. This is consistent with the prior discussion about the role of the ion bombardment energy.

Both sample sets (A-RF and C-RF) show an increase in the percentage of sp^2 hybridized carbon bonding, from XAES results, as the RF power increases (plot not shown here). The C-RF sample set possesses much greater sp^2 bonding than the A-RF sample set as indicated in Fig. 5. The percentage of sp^2 hybridization increases as the RF power increases due to large ion energy impinging on the film and the low film density. High energy ions process enough energy to overcome the penetration threshold energy of the film, i.e. 32 eV. The excess energy that these ions possess, above the threshold energy, will be transferred to the thermal energy to the film. This relaxes C – C sp^3 bonds to the more stable C – C sp^2configuration [19], leading to a further increase in %sp^2 bonding of the film. The rapid increase in the % sp^2 for the C-RF samples compared to A-RF ones is due to the much larger ion energy impinging on the cathode.

Robertson [19] describes the microstructures of a-C as a continuous network of sp^3 bonded carbon atoms with sp^2 bonded carbon localized clusters embedded within the network. The sp^3 bond configuration forms σ–σ* bands and the sp^2 sites creates π–π* bands which form localized states. The size and quantity of the sp^2 clusters dominates the film's optical properties. Accordingly, the increasing % sp^2 in the film implies an increase in the localized density of states lying deeper in the gap. This leads to the decrease in E_{04} bandgap and the increase in extinction coefficient as illustrated in Fig. 5.

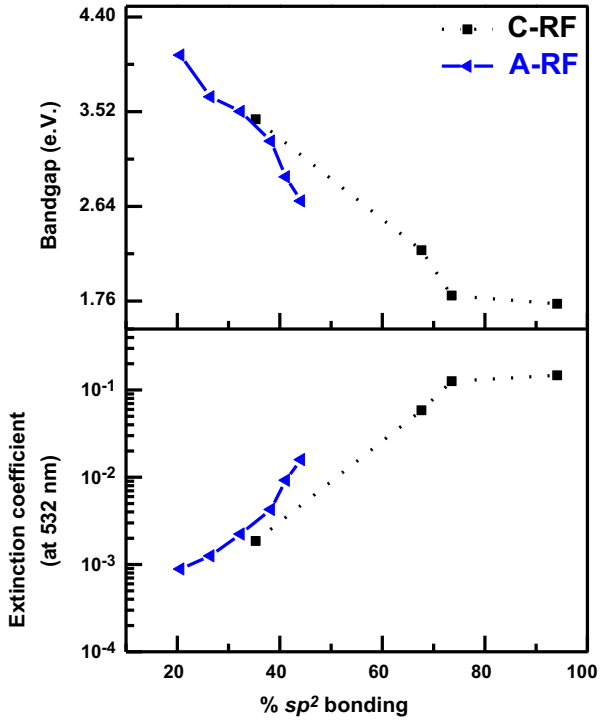

Fig. 5. The optical bandgap E_{04} and extinction coefficient k at 532 nm of the a-C:H films grown on the anode (solid line), and cathode (dash line), as a function of the % sp^2 bonding.

3.2. a-C:H (Er) PL

As discussed above, the host a-C:H films deposited on the anode exhibit a wider bandgap and less % of sp^2 carbon bonding. Thus the host film absorption in 1540 nm wavelength range is expected to be minimized. Hence, the substrates were situated on the anode while performing the in-situ doping using the Er(fod)$_3$ compound to synthesize the a-C:H(Er) film.

The room temperature PL spectrum centered at 1540 nm exhibited in Fig. 6(a) corresponds to the $^4I_{13/2}$ to $^4I_{15/2}$ electronic transition of Er^{3+} ions. The spectral width of the emission band is due to inhomogeneous and homogeneous broadening in addition to Stark splitting of the Er^{3+} excited and ground states. The PL peak is wider than that of other Er-implanted silicate glasses [8], indicating the Er^{3+} possesses a variety of local bonding environments in the a-C:H matrix. Its 65 nm of full width at half-maximum (FWHM) suggests the potential of enabling a wide gain band width for optical amplification. From XPS analysis, the concentration of Er of a-C:H(Er) film is estimated to be 3.9 at.%, which is much higher than those prepared by magnetron sputtering [15,16], pulsed laser deposition [28,29], and DC Saddle-Field PECVD [17]. Furthermore, the depth distribution depicted in Fig. 6(b) reveals a uniform concentration of Er throughout the film (thickness of 850 nm). This contrasts the ion-implantation of Er where the optically active ions are always located near the surface [8]. Note that the high oxygen at the surface is simply surface contamination.

The prominent PL signal observed from the a-C:H(Er) film is attributed to several factors including a high Er concentration, the large optical bandgap of the a-C:H host, and the decrease in the C – H quenching. The long hydrocarbon ligands of the Er metalorganic compound matches the internal structure of the a-C:H host matrix. This is thought to result in a high solubility of the Er metalorganic compound, and hence promote a high Er concentration. The large optical bandgap of the a-C:H host is thought to increase the pumping efficiency of the Er^{3+} ions without high absorption from a-C:H host itself. To effectively

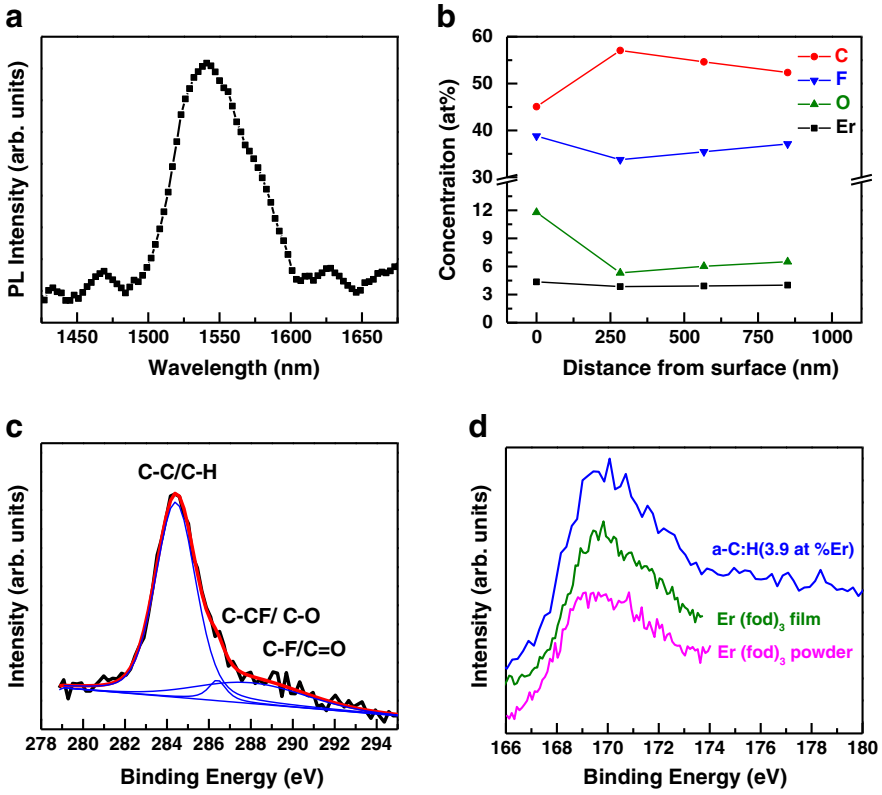

Fig. 6. (a) Room-temperature PL spectrum of a-C:H(Er) with peak centered at 1540 nm and FWHM of ~65 nm. (b) Depth profile of C, F, O, and Er concentrations from XPS measurements. (c) Deconvoluted XPS C1s spectrum of the a-C:H(Er) film. (d) XPS Er4d spectra of a-C:H(Er) film, Er(fod)$_3$ film (evaporated in the vacuum chamber with CH_4 precursor gas flowing without plasma ignition), and Er (fod)$_3$ powder.

decrease the C – H quenching, partial fluorination is incorporated into the a-C:H(Er) film from the Er metalorganic compound.

The ratio of the O to Er concentration in the a-C:H(Er) film is approximately 1.5 in the film instead of 6 in the pristine Er(fod)$_3$ compound. Table 1 lists the ratio of the atomic concentrations and the relative (and the absolute) atomic concentrations of the Er(fod)$_3$ compound, thermally evaporated Er(fod)$_3$, and the a-C:H(Er) form XPS measurements. The [F]/[O], [C]/[O], and [C]/[F] concentration ratios are approximately 5.9, 9.1, and 1.5, which is greater than the Er(fod)$_3$ stoichiometric ratios of 3.5, 5, and 1.4. However, the [F]/[Er] and [C]/[Er] concentration ratios are approximately 9 and 14, all less than the Er(fod)$_3$ stoichiometric ratios of 21 and 30. This implies that the plasma causes significant dissociation of the Er(fod)$_3$ metalorganic compound. It is noted that the thermally evaporated Er(fod)$_3$ film possesses essentially the same relative concentration as the Er(fod)$_3$ compound, with the exception that the [C] is enhanced. The [F]/[O], [F]/[Er], and [O]/[Er] ratios are similar, while the [C]/[O], [C]/[F], and [C]/[Er] are much larger than the stoichiometric Er(fod)$_3$ compound. This increase in the [C] is thought to be due to the trapping or intermolecular bonding of methane like species in the Er(fod)$_3$ film.

For the a-C:H(Er) film, Fig. 6(c) displays the C1s XPS spectra indicating the majority of carbon bonds are C – C and C – H, with some C – F, and a few C – O bonds. Although, relative to [Er], the concentrations of O, F, and C have decreased in descending order ([C] has decreased the least with respect to [Er]). This is witnessed by the greater [F]/[O], [C]/[O], and [C]/[F] ratios. It is surprising that the [C]/[Er] ratio has decreased, since CH_x (x = 0…3) radicals/ions are also being deposited by the methane plasma. Although this could be due to the loss of large organic fragments since the concentration of all species relative to Er is lower (when compared to the Er(fod)$_3$ power or film). However, the relative (as [H] is unknown) atomic concentration of F is high. This may indicate that part of the molecule (C_mF_7, m > 5) accounts for a significant fraction of the film. This is a positive result, since the Er(fod)$_3$ compound was selected for the purposes of incorporating the large fluorinated ligands into the a-C:H matrix. With respect to the change in film properties after Er metalorganic compound incorporation, the % sp^2 bonding of the a-C:H(Er) film is expected to increase compared to that in the a-C:H host due to the addition of Er dopant in the carbon matrix based on the observations from Foong et al. [28,29]. In addition, with the high fraction of fluoride composites, as analyzed from XPS measurement, the % sp^2 bonding would be expected to be further enhanced as demonstrated previously [30–32]. Accordingly, a decrease in the optical bandgap E_{04} and an increase in the extinction coefficient k of the film would occur. The detailed optical properties of the a-C:H(Er) film are still under investigation.

One obvious result is that oxygen is being reduced or omitted from the a-C:H(Er) film. This is clearly seen through the elevated

Table 1
The ratio of the atomic concentrations and the relative/absolute atomic concentrations of the Er(fod)$_3$ compound, thermally evaporated Er(fod)$_3$, and the a-C:H(Er) film from XPS measurements.

	C at.%	F at.%	O at.%	Er at.%	[F]/[O]	[C]/[O]	[C]/[F]	[F]/[Er]	[C]/[Er]	[O]/[Er]
$Er(C_{10}H_{10}F_7O_2)_3$	34.1[a]	23.9[a]	6.8[a]	1.1[a]	3.5	5.0	1.4	21.0	30.0	6.0
Er(fod)$_3$thermal evaporated film	71.3	21.5	6.3	1.0	3.4	11.4	3.3	21.7	72.1	6.3
a-C:H(Er) film	54.6	35.4	6.0	3.9	5.9	9.1	1.5	9.0	13.9	1.5

[a] The absolute atomic concentrations.

concentrations of C, F, and Er relative to oxygen. Although, the observance of a PL signal indicates that some of the erbium is in the 3+ state. Fig. 6(d) shows the XPS Er4d spectra for the a-C:H(Er) film, $Er(fod)_3$ evaporated film, and the $Er(fod)_3$ powder. The three spectra are similar indicating that the local bonding environments are also similar. That is, oxygen is bonded to the erbium in the correct configuration. Moreover, the proximity of the C – H bonds is thought to be far enough from Er^{3+} ions to avoid quenching. However, the optimization of the process and the electronic transfer mechanism are still under investigation.

4. Conclusion

The feasibility of the in-situ growth of Er-doped a-C thin films (a-C:H(Er)) on Si substrates at low temperature (<200 °C) by a simple one-step MO-RFPECVD system was demonstrated. A high Er concentration (3.9 at.%) in a-C:H(Er) films was achieved and room-temperature photoluminescence peaking at 1.54 μm was observed. By adopting an Er metalorganic precursor, $Er(fod)_3$, the optically active Er^{3+} ions are preserved without the need for any subsequent high temperature annealing. Furthermore, the in-situ thermal evaporation technique provides the potential of doping Er in a vertically uniform profile. In addition, non-radiative C – H vibrational quenching was significantly reduced by partial fluorination of the surrounding ligands. This was achieved despite the use of hydrogenated amorphous carbon as the host material.

Acknowledgments

This work was supported by the Natural Sciences and Engineering Research Council of Canada (NSERC) Discovery grants, the NSERC CREATE program in Nanoscience and Nanotechnology, and the Departments of Electrical and Computer Engineering at the University of Toronto and Materials Science and Engineering at the University of Toronto. The authors also acknowledge valuable discussions with Dr. Rana Sodhi for the analysis of XPS results, and help from Dr. Davit Yeghikyan and Dr. Tome Kosteski for the assembly of the MO RF-PECVD system.

References

[1] M. Paniccia, Integrating silicon photonics, Nat. Photonics 4 (2010) 498.
[2] L. Pavesi, L. Dal Negro, C. Mazzoleni, G. Franzo, F. Priolo, Optical gain in silicon nanocrystals, Nature 408 (2000) 440.
[3] M.A. Green, J. Zhao, A. Wang, P.J. Reece, M. Gal, Efficient silicon light-emitting diodes, Nature 412 (2001) 805.
[4] R.J. Walters, G.I. Bourianoff, H.A. Atwater, Field-effect electroluminescence in silicon nanocrystals, Nat. Mater. 4 (2005) 143.
[5] H. Rong, A. Liu, R. Jones, O. Cohen, D. Hak, R. Nicolaescu, A. Fang, M. Paniccia, An all-silicon Raman laser, Nature 433 (2005) 292.
[6] Q. Xu, B. Schmidt, S. Pradhan, M. Lipson, Micrometre-scale silicon electro-optic modulator, Nature 435 (2005) 325.
[7] G. Weiser, H. Kühne, I.E. Terukov, Energy transfer to Er^{3+} ions in a-$Si_{1-x}C_x$:H alloys: emission at 1.54 mm wavelength, Phys. Status Solidi C 1 (2004) 1275.
[8] A. Polman, Erbium implanted thin film photonic materials, J. Appl. Phys. 82 (1997) 1.
[9] H. Ennen, J. Schneider, G. Pomrenke, A. Axmann, 1.54 μm luminescence of erbiumimplanted IIIV semiconductors and silicon, Appl. Phys. Lett. 43 (1983) 943.
[10] M. Miritello, R. Lo Savio, F. Iacona, G. Franzò, A. Irrera, A.M. Piro, C. Bongiorno, F. Priolo, Efficient luminescence and energy transfer in erbium silicate thin films, Adv. Mater. 19 (2007) 1582.
[11] A. Polman, G.N.v.d. Hoven, J.S. Custer, J.H. Shin, R. Serna, P.F.A. Alkemade, Erbium in crystal silicon: optical activation, excitation, and concentration limits, J. Appl. Phys. 77 (1995) 1256.
[12] S. Coffa, G. Franzò, F. Priolo, A. Polman, R. Serna, Temperature dependence and quenching processes of the intra-4f luminescence of Er in crystalline Si, Phys. Rev. B 49 (1994) 16313.
[13] S. Coffa, F. Priolo, G. Franzo, V. Bellani, A. Carnera, C. Spinella, Optical activation and excitation mechanisms of Er implanted in Si, Phys. Rev. B 48 (1993) 11782.
[14] A.M. Baranov, V.V. Sleptsov, A.A. Nefedov, A.E. Varfolomeev, S.S. Fanchenko, L. Calliari, G. Speranza, M. Ferrari, A. Chiasera, Erbium photoluminescence in hydrogenated amorphous carbon, Phys. Status Solidi B 234 (2002) R1.
[15] G. Speranza, L. Calliari, M. Ferrari, A. Chiasera, K. Tran Ngoc, A.M. Baranov, V.V. Sleptsov, A.A. Nefedov, A.E. Varfolomeev, S.S. Fanchenko, Erbium-doped thin amorphous carbon films prepared by mixed CVD sputtering, Appl. Surf. Sci. 238 (2004) 117.
[16] V. Prajzler, I. Huttel, P. Nekvindova, J. Schrofel, A. Mackova, J. Gurovic, Erbium doping into thin carbon optical layers, Thin Solid Films 433 (2003) 363.
[17] R.Y.C. Tsai, L. Qian, H. Alizadeh, N.P. Kherani, Room-temperature photoluminescence in erbium-doped deuterated amorphous carbon prepared by low-temperature MO-PECVD, Opt. Express 17 (2009) 21098.
[18] P. Patsalas, Optical properties of amorphous carbons and their applications and perspectives in photonics, Thin Solid Films 519 (2011) 3990.
[19] J. Robertson, Diamond-like amorphous carbon, Mater. Sci. Eng. R 37 (2002) 129.
[20] F. Piazza, D. Grambole, D. Schneider, C. Casiraghi, A.C. Ferrari, J. Robertson, Protective diamond-like carbon coatings for future optical storage disks, Diam. Relat. Mater. 14 (2005) 994.
[21] J.A. McLaughlin, P.D. Maguire, Advances on the use of carbon based materials at the biological and surface interface for applications in medical implants, Diam. Relat. Mater. 17 (2008) 873.
[22] C. Piamonteze, L.R. Tessler, H. Tolentino, M.d.C.M. Alves, G.W. Alves, E. Terukov, Er environment in a-Si:H(Er) prepared by PECVD, Mat. Res. Soc. Symp. Proc. 609 (2000) A11.2.1.
[23] A. Monguzzi, R. Tubino, F. Meinardi, A.O. Biroli, M. Pizzotti, F. Demartin, F. Quochi, F. Cordella, M.A. Loi, Novel Er^{3+} perfluorinated complexes for broadband sensitized near infrared emission, Chem. Mater. 21 (2008) 128.
[24] K. Kuriki, Y. Koike, Y. Okamoto, Plastic optical fiber lasers and amplifiers containing lanthanide complexes, Chem. Rev. 102 (2002) 2347.
[25] A.R. Forouhi, I. Bloomer, Optical dispersion-relations for amorphous-semiconductors and amorphous dielectrics, Phys. Lett. B 34 (1986) 7018.
[26] J. Ristein, R.T. Stief, L. Ley, W. Beyer, A comparative analysis of a-C:H by infrared spectroscopy and mass selected thermal effusion, J. Appl. Phys. 84 (1998) 3836.
[27] J.C. Lascovich, V. Rosato, Analysis of the electronic structure of hydrogenated amorphous carbon via Auger spectroscopy, Appl. Surf. Sci. 152 (1999) 10.
[28] Y.M. Foong, J. Hsieh, X. Li, D.H.C. Chua, Comparative study between erbium and erbium oxide-doped diamondlike carbon films deposited by pulsed laser deposition technique, J. Vac. Sci. Technol. A 28 (2010) 449.
[29] Y.M. Foong, J. Hsieh, X. Li, D.H.C. Chua, The study on the effect of erbium on diamond-like carbon deposited by pulsed laser deposition technique, J. Appl. Phys. 106 (2009) 064904.
[30] M.H. Ahmed, J.A. Byrne, J. McLaughlin, Evaluation of glycine adsorption on diamond like carbon (DLC) and fluorinated DLC deposited by plasma-enhanced chemical vapour deposition (PECVD), Surf. Coat. Technol. 209 (2012) 8.
[31] A. Bendavid, P.J. Martin, L. Randeniya, M.S. Amin, R. Rohanizadeh, The properties of fluorine-containing diamond-like carbon films prepared by pulsed DC plasma-activated chemical vapour deposition, Diam. Relat. Mater. 19 (2010) 1466.
[32] S.F. Ahmed, D. Banerjee, K.K. Chattopadhyay, The influence of fluorine doping on the optical properties of diamond-like carbon thin films, Vacuum 84 (2010) 837.